Journal of Molecular Structure 1237 (2021) 130346

Contents lists available at ScienceDirect

Journal of Molecular Structure

journal homepage: www.elsevier.com/locate/molstr

Novel pyrano-triazolo-pyrimidine derivatives as anti- α-amylase agents: Synthesis, molecular docking investigations and computational analysis

Amel Hajlaoui[a], Maha Laajimi[b], Mansour Znati[a], Hichem Ben Jannet[a], Anis Romdhane[a,*]

[a] University of Monastir, Faculty of Sciences of Monastir, Laboratory of Heterocyclic Chemistry, Natural Products and Reactivity (LR11ES39), Team: Medicinal Chemistry and Natural Products, Avenue of Environment, 5019 Monastir, Tunisia
[b] Quantum and Statistical Physics Laboratory, Faculty of Sciences, University of Monastir, Monastir, Tunisia

ARTICLE INFO

Article history:
Received 18 January 2021
Revised 21 February 2021
Accepted 19 March 2021
Available online 26 March 2021

Keywords:
Pyranotriazolopyrimidine
α-amylase inhibition
In *silico* docking study
Pharmacokinetics
HOMO-LUMO energy

ABSTRACT

A novel series of pyranotriazolopyrimidine derivatives **3a-j** was synthesized and characterized by ^{1}H NMR, ^{13}C NMR, and HRMS experimental data. The synthesized compounds were assessed for their inhibitory potential on the α-amylase enzyme. Results showed that seven of the synthesized compounds displayed potent α-amylase inhibitory activity. Compound **3b** (IC_{50} = 2.78 ± 0.14 μg/mL) bearing a cyanomethyl group at triazole ring, exhibited the highest activity followed by **2a, 2b** and **3c** with IC_{50} values ranging from 3.15 ± 0.25 to 4.15 ± 0.10 μg/mL, in comparison to the standard acarbose IC_{50} = 6.84 ± 1.22 μg/mL). A molecular docking study was performed to investigate the possible inhibitory mechanism at the binding site of the target enzyme which reinforced the observed activity of compounds **2a, 2b, 3b**, and **3c**. The analysis revealed the strength of intermolecular hydrogen bonding and hydrophobic interactions in the ligand-receptor complexes as significant descriptors to rationalize the inhibition results obtained. Several physicochemical properties related to the pharmacokinetics of the synthesized derivatives were predicted. These properties were found to lie within the desired limit and we have noticed that all compounds are likely to be orally active as they obeyed Lipinski's rule of five. HOMO-LUMO energy gap and some reactivity descriptor's parameters were evaluated using Density Functional Theory (DFT) employing B3LYP level with 6-311++G (d,p) basis set.

1. Introduction

Type 2 Diabetes mellitus (T2DM) is a metabolic disorder characterized by high blood sugar levels over a prolonged period. Uncontrolled hyperglycemia can cause serious damage to many vital organs such as heart disease, kidney damage and nerve damage [1]. A therapeutic approach for treating diabetes in its early stages is to reduce postprandial hyperglycemia. This is done by retarding glucose absorption through the inhibition of the carbohydrate-hydrolyzing enzymes, α-amylase and α-glucosidase, in the digestive tract [2,3]. Particularly, α-amylase, is one of the enzymes of great concern to the medical practitioners and researchers in the control of T2DM. Inhibitors of this enzyme lead to a reduction in the glucose absorption rate and, therefore, attenuate the postprandial glucose levels [4]. Acarbose and miglitol are such oral hypoglycemic drugs. These inhibitors present certain limitations due to their side effects, such as abdominal discomfort, diarrhea, and meteorism [5,6]. Thus, it is necessary to develop new and safe therapeutic agents with low side effects to treat type 2 diabetes.

Researchers are now focused on finding new heterocyclic moieties that, if studied systematically, may appear to be potential candidates for glycosidase inhibitors.

Due to their exceptional chemical and versatile biological profiles, heterocyclic systems are considered as an attractive area for most medicinal chemists and have therefore been the privileged core of the majority of medicinal compounds [7]. Among these heterocycles, pyrimidine and triazole rings, which have played a crucial role in several biological processes and have had a considerable pharmacological and chemical importance as anticancer, anti-alzheimer, antifungal, antihypertensive, analgesic and potential herbicidal activities [8,9]. These compounds have frequently proven their efficiency in different fields of medicinal drug, biochemistry, materials science, and agrochemistry [10–12].

Another one of relevance building blocks in the design of bioactive structures is 4*H*-Pyran ring [13]. Indeed, pyrans and their derivatives constitute a promising class of oxygen-containing heterocyclic compounds, which have shown a broad series of biological

* Corresponding author.

https://doi.org/10.1016/j.molstruc.2021.130346
0022-2860/

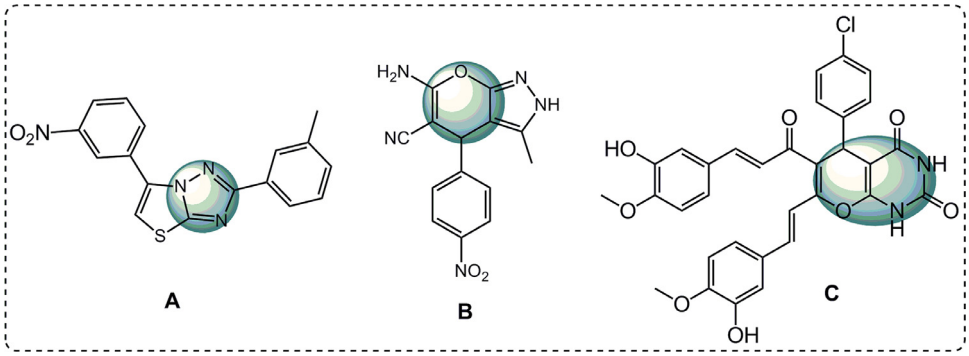

Fig. 1. Previously reported antidiabetic compounds.

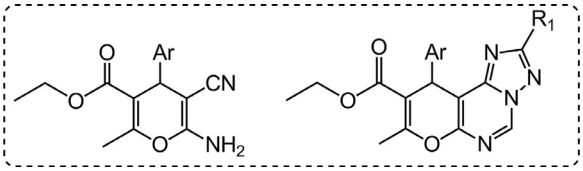

Fig. 2. The starting reagent and target compounds.

effects, including antitumor [14], anticoagulant [15] and anti-alzheimer [16] activities. These derivatives have been found in diverse biodegradable agrochemicals, pigments, fluorescent reagents, and photo-active materials [17,18]. It is also important to note that pyran, triazole, and pyrimidine have been reported to exhibit potential antidiabetic activity [10,19]. In this regard, Channar et al [20] prepared a series of 1,2,4-triazole derivatives that have shown promising results against α-amylase, among them compound **A** (Fig. 1) has demonstrated a strong α-amylase inhibitory activity (IC_{50} = 1.1 mmol/g) [19]. Likewise, compound **B** has been identified as a potent anti-diabetic analog with an IC_{50} value of 54.2 ± 2.02 µM [21]. Fused pyrimidines have also been studied as inhibitors for α-amylase such as compound **C,** showing a percentage inhibition value of 92% [22].

In the light of these findings, it was considered worthwhile to synthesize a new condensed pyrimidine scaffold using an efficient and convenient synthetic method: the multicomponent reaction. This latter has been presented as a powerful and remarkable synthetic approach in the preparation of heterocyclic components owing to its simple experimentations and its high atom economy [23]. Thus, we report in this paper the use of α-aminocarbonitriles **1** as starting material for the synthesis of a new series of pyranotriazolopyrimidines **3** (Fig. 2). Computational approaches were carried out to explain some pharmacokinetic effects of compounds (**1, 2** and **3**) as well as certain toxicological properties. These compounds were tested for their *in vitro* α-amylase inhibitory activity. *In silico* studies were performed to gain insight toward the interactions of title compounds with the target protein α-amylase. The HOMO-LUMO energy gap and some reactivity descriptor's parameters were evaluated to simulate the electronic properties of our compounds through DFT calculations using B3LYP 6-311++G(d,p) method.

2. Experimental section

2.1. Chemistry

Progress of the reactions was monitored by Thin Layer Chromatography (TLC) using aluminum sheets of Merck silica gel 60 F254, 0.2 mm. Column chromatography was carried out on silica gel (70-230 mesh) using chloroform and ethyl acetate mixture as eluents. Melting points are uncorrected and were determined using an electrothermal 9002 apparatus. ^{1}H (300 MHz) and ^{13}C (75 MHz) NMR spectra were recorded on a Bruker AC-300 spectrometer, in deuterated $CDCl_3$ and DMSO-d_6 using non-deuterated solvents as an internal standard. Chemical shifts (δ) are expressed in ppm and coupling constants (J) in Hz. High-Resolution Mass Spectra (HRES- MS) were obtained with Micromass LCT (ESI technique, positive mode) spectrometers.

2.1.1. General procedure for the synthesis of 2-amino-3-cyanopyranes (1)

A mixture of arylaldehyde (10 mmol), malononitrile (10 mmol), ethyl acetoacetate (10 mmol) and a catalytic amount of piperidine was stirred in 30 mL of absolute ethanol at room temperature for 1 h. The solid product obtained was filtered, dried, and purified by recrystallization from ethanol to afford compounds **1a-c**.

*2.1.1.1. 2-amino-3-cyano-5-ethoxycarbonyl-6-methyl-4-phenyl-4H-pyran (**1a**).* White solid, yield: 70%, mp: 194-196°C, ^{1}H NMR (DMSO-d_6, 300 MHz): δ (ppm) = 1.03 (t, 3H, H9, J= 5.2 Hz); 2.32 (s, 3H, H10); 3.97 (q, 2H, H8, J= 5.2 Hz); 4.30 (s, 1H, H4); 6.90 (s, 2H, NH_2); 7.14 - 7.33 (m, 5H, Harom). ^{13}C NMR (DMSO-d_6, 75 MHz): δ (ppm) = 14.2 (C9); 18.6 (C10); 39.3 (C4); 57.8 (C3); 60.6 (C8); 107.6 (C5); 120.2 (CN); 127.3 (C4'); 127.7 (C2', 6'); 128.9 (C3', 5'); 145.2 (C1'); 157.0 (C6); 158.9 (C2); 165.9 (C7). HR-ES-MS $[M+H]^+$ calcd for $(C_{16}H_{17}N_2O_3)^+$: 285.1161, found: 285.1194.

*2.1.1.2. 2-amino-3-cyano-5-ethoxycarbonyl-6-methyl-4-(4-methoxyphenyl)-4H-pyran (**1b**).* White solid, yield: 81%, mp: 130-132°C. ^{1}H NMR (DMSO-d_6, 300 MHz): δ (ppm) = 1.13 (t, 3H, H9, J= 5.3 Hz); 2.37 (s, 3H, H10); 3.78 (s, 3H, H11); 4.05 (q, 2H, H8, J= 5.3 Hz); 4.42 (s, 1H, H4); 4.54 (s, 2H, NH_2); 6.84 (d, 2H, H3′, 5′, J= 6.4 Hz); 7.13 (d, 2H, H2′, 6′, J= 6.4 Hz). ^{13}C NMR (DMSO-d_6, 75 MHz): δ (ppm) = 14.0 (C9); 18.4 (C10); 38.0 (C4); 55.3 (C11); 60.7 (C3); 62.5 (C8); 108.2 (C5); 119.1 (CN); 114.0 (C3', 5'); 128.6 (C2', 6'); 136.1 (C1'); 156.3 (C6); 157.4 (C4′); 158.7 (C2); 166.0 (C7). ES-MS $[M+H]^+$ calcd for $(C_{17}H_{19}N_2O_4)^+$: 315.1267, found: 315.13.

*2.1.1.3. 2-amino-4-(4-chlorophenyl)-3-cyano-5-ethoxycarbonyl-6-methyl-4H-pyran (**1c**).* White solid, yield: 79%, mp: 177-179°C. ^{1}H NMR ($CDCl_3$, 300 MHz): δ (ppm) = 1.13 (t, 3H, H9, J= 5.3 Hz); 2.37 (s, 3H, H10); 4.05 (q, 2H, H8, J= 5.3 Hz); 4.44 (s, 1H, H4); 4.62 (s, 2H, NH_2); 7.15 (d, 2H, H2′, 6′, J= 6.3 Hz); 7.28 (d, 2H, H3′, 5′, J= 6.3 Hz). ^{13}C NMR ($CDCl_3$, 75 MHz): δ (ppm) = 13.8 (C9); 18.5 (C10); 38.2 (C4); 60.7 (C3); 61.5 (C8); 107.6 (C5); 118.7 (CN); 128.8 (C2', 6'); 129.0 (C3', 5'); 133.0 (C4'); 142.4 (C1'); 157.0 (C6); 157.6 (C2); 165.7 (C7). ES-MS $[M+H]^+$ calcd for $(C_{16}H_{16}ClN_2O_3)^+$: 319.0771, found: 319.0782.

2.1.2. General procedure for the synthesis of iminoethers 2

The mixture of 1 mmol of pyranic derivative **1** and 1 mmol of triethylorthoformate was added to 25 mL of acetic anhydride and refluxed for 6 hours. After cooling, the resulting product was filtered and throughly washed with petroleum ether to provide compounds **2a-c.**

*2.1.2.1. Ethyl 5-cyano-6-((ethoxymethylene)amino)-2-methyl-4-phenyl-4H-pyran-3-carboxylate (**2a**).* White solid, yield: 79%, mp: 94-96°C. ^{1}H NMR (DMSO-d_6, 300 MHz): δ (ppm) = 1.03 (t, 3H, H9, J= 5.3 Hz); 1.30 (t, 3H, H13, J= 5.3 Hz); 2.36 (s, 3H, H10); 3.98 (q, 2H, H8, J= 5.3 Hz); 4.30 (q, 2H, H12, J= 5.3 Hz); 4.52 (s, 1H, H4); 7.23 - 7.38 (m, 5H, Harom); 8.54 (s, 1H, H11). ^{13}C NMR (DMSO-d_6, 75 MHz): δ (ppm) = 14.0 (CH_3); 14.1 (CH_3); 18.6 (C10); 39.2 (C4); 60.6 (C8); 64.5 (C12); 81.7 (C3); 106.6 (C5); 117.7 (CN); 127.9 (C4'); 128.2 (C2', 6'); 129.1 (C3', 5'); 143.5 (C1'); 156.3 (C6); 157.7 (C11); 162.3 (C2); 165.7 (C7). ES-MS $[M+H]^+$ calcd for $(C_{19}H_{21}N_2O_4)^+$: 341.144, found: 341.151.

*2.1.2.2. Ethyl 5-cyano-6-((ethoxymethylene)amino)-4-(4-methoxyphenyl)-2-methyl-4H-pyran-3-carboxylate (**2b**).* White solid, yield: 69%, mp: 152-154°C. ^{1}H NMR ($CDCl_3$, 300 MHz): δ (ppm) = 1.14 (t, 3H, H9, J= 7.2 Hz); 1.37 (t, 3H, H13, J= 7.2 Hz); 2.41 (s, 3H, H10); 3.79 (s, 3H, H14); 4.07 (q, 2H, H8, J= 7.2 Hz); 4.38 (q, 2H, H12, J= 7.2 Hz); 4.53 (s, 1H, H4); 6, 85 (d, 2H, H3′,5′, J= 8.7 Hz); 7, 17 (d, 2H, H2′,6′, J= 8.7 Hz); 8, 23 (s, 1H, H11). ^{13}C NMR ($CDCl_3$, 75 MHz): δ (ppm) = 13.4 (CH_3); 13.5 (CH_3); 17.9 (C10); 39.3-39.4 (C4, C14); 60.2 (C8); 63.7 (C12); 82.6 (C3); 106.5 (C5); 113.5 (C3', 5'); 116.9 (CN); 128.4 (C2', 6'); 134.5 (C1'); 154.9 (C6); 156.8 (C11); 158.4 (C2); 158.5 (C4'); 165.4 (C7). ES-MS $[M+H]^+$ calcd for $(C_{20}H_{23}N_2O_3)^+$: 371.1529, found: 371.1622.

*2.1.2.3. Ethyl 4-(4-chlorophenyl)-5-cyano-6-((ethoxymethylene) amino)-2-methyl-4H-pyran-3-carboxylate (**2c**).* White solid, yield: 71%, mp: 95-97°C. ^{1}H NMR (DMSO-d_6, 300 MHz): δ (ppm) = 1.04 (t, 3H, H9, J= 5.3 Hz); 1.29 (t, 3H, H13, J= 5.3 Hz); 2.37 (s, 3H, H10); 3.98 (q, 2H, H8, J= 5.3 Hz); 4.30 (q, 2H, H12, J= 5.3 Hz); 4.56 (s, 1H, 1H, H4); 7.27 (d, 2H, H2′, 6′, J= 6.3 Hz); 7, 42 (d, 2H, H3′, 5′, J= 6.3 Hz); 8.54 (s, 1H, H11). ^{13}C NMR (DMSO-d_6, 75 MHz): δ (ppm) =14.1 (CH_3); 14.2 (CH_3); 18.6 (C10); 39.3 (C4); 60.8 (C8); 64.5 (C12); 81.2 (C3); 106.1 (C5); 117.5 (CN); 129.1 (C2', 6'); 130.1 (C3', 5'); 132.5 (C4'); 142.5 (C1'); 156.5 (C6); 158.2 (C11); 162.5 (C2); 165.5 (C7). ES-MS $[M+H]^+$ calcd for $(C_{19}H_{20}ClN_2O_4)^+$: 375.1033, found: 375.1043.

*2.1.3. General procedure for the synthesis of pyrimidine derivatives **3***

0.7 mmol of iminoether **2** and 1.2 equivalents of hydrazide were refluxed in dry dioxane (20 mL) in the presence of a few drops of acetic acid. The solid formed by precipitation was filtered, washed with petroleum ether, dried and purified by column chromatography ($CHCl_3$ /AcOEt: 9/1) to yield the compounds **3**.

*2.1.3.1. Ethyl 8-methyl-2,10-diphenyl-10H-pyrano[3,2-e][1,2,4]triazolo [1,5-c]pyrimidine-9-carboxylate (**3a**).* White solid, yield: 67%, mp: 220-222°C. ^{1}H NMR ($CDCl_3$, 300 MHz): δ (ppm) = 1.21 (t, 3H, H13, J= 7.1 Hz); 2.65 (s, 3H, H14); 4.16 (q, 2H, H12, J= 7.1 Hz); 5.61 (s, 1H, H10); 7.18 - 8.29 (m, 10H, Harom); 9.04 (s, 1H, H5). ^{13}C NMR ($CDCl_3$, 75 MHz): δ (ppm) = 14.0 (C13); 19.0 (C14); 37.9 (C10); 60.7 (C12); 104.0 (C9); 106.9 (C10a); 127.2 (C4'); 127.8 (C2'', 6''); 128.3 (C3', 5'); 128.5 (C2', 6'); 128.7 (C3'', 5''); 129.8 (C4''); 130.8 (C1''); 138.2 (C5); 142.7 (C1'); 152.7 (C10b); 153.1 (C8); 159.9 (C2); 165.9 (C6a); 167.2 (C11). ES-MS $[M+H]^+$ calcd for $(C_{24}H_{21}N_4O_3)^+$: 413.1554, found: 413.1620.

*2.1.3.2. Ethyl 2-(cyanomethyl)-8-methyl-10-phenyl-10H-pyrano[3,2-e][1,2,4]triazolo[1,5-c]pyrimidine-9-carboxylate (**3b**).* Orange solid, yield: 58%, mp: 164-166°C. ^{1}H NMR ($CDCl_3$, 300 MHz): δ (ppm) = 1.21 (t, 3H, H13, J= 5.3 Hz); 2.63 (s, 3H, H14); 4.01 (s, 2H, H15); 4.13 (q, 2H, H12, J= 5.3 Hz); 5.50 (s, 1H, H10); 7.18 - 7.44 (m, 5H, Harom); 9.05 (s, 1H, H5). ^{13}C NMR ($CDCl_3$, 75 MHz): δ (ppm) = 14.0 (C13); 18.7 (C14); 19.0 (C15); 37.8 (C10); 60.8 (C12); 104.3 (C9); 107.1 (C10a); 114.6 (CN); 127.5 (C4'); 128.4 (C3', 5'); 128.5 (C2', 6'); 138.2 (C5); 142.3 (C1'); 153.2 (C2); 153.3 (C10b); 159.7 (C8); 160.6 (C6a); 165.6 (C11). ES-MS $[M+H]^+$ calcd for $(C_{20}H_{18}N_5O_3)^+$: 376.1345, found: 376.1419.

*2.1.3.3. Ethyl 2,8-dimethyl-10-phenyl-10H-pyrano[3,2-e][1,2,4]triazolo [1,5-c]pyrimidine-9-carboxylate (**3c**).* White solid, yield: 61%, mp: 172-174°C. ^{1}H NMR ($CDCl_3$, 300 MHz): δ (ppm) = 1.21 (t, 3H, H13, J= 6.9 Hz); 2.07 (s, 3H, H15); 2.16 (s, 3H, H14); 4.13 (q, 2H, H12, J= 6.9 Hz); 5.57 (s, 1H, H10); 7.17 - 7.50 (m, 5H, Harom); 8.97 (s, 1H, H5). ^{13}C NMR ($CDCl_3$, 75 MHz): δ (ppm) = 14.5 (CH_3); 19.0 (CH_3); 37.2 (C14); 37.6 (C10); 60.3 (C12); 103.5 (C9); 107.3 (C10a); 127.7 (C4'); 128.1 (C3', 5'); 128.4 (C2', 6'); 137.6 (C5); 142.7 (C1'); 152.5 (C10b); 153.0 (C2); 159.8 (C8); 165.7 (C6a); 167.1 (C11). ES-MS $[M+H]^+$ calcd for $(C_{19}H_{19}N_4O_3)^+$: 351.138, found: 351.148.

*2.1.3.4. Ethyl 8-methyl-10-phenyl-10H-pyrano[3,2-e][1,2,4]triazolo [1,5-c]pyrimidine-9-carboxylate (**3d**).* White solid, yield: 54%, mp: 120-122°C. ^{1}H NMR ($CDCl_3$, 300 MHz): δ (ppm) = 1.22 (t, 3H, H13, J= 6.9 Hz); 2.63 (s, 3H, H14); 4.14 (q, 2H, H12, J= 6.9 Hz); 5.55 (s, 1H, H10); 7.17 - 7.47 (m, 5H, Harom); 8.30 (s, 1H, H2); 9.10 (s, 1H, H5). ^{13}C NMR ($CDCl_3$, 75 MHz): δ (ppm) = 13.5 (C13); 18.5 (C14); 37.5 (C10); 60.3 (C12); 103.1 (C9); 106.7 (C10a); 126.8 (C4'); 127.9 (C3', 5'); 128.4 (C2', 6'); 138.1 (C5); 142.1 (C1'); 151.7 (C10b); 152.4 (C2); 156.3 (C8); 159.1 (C6a); 165.3 (C11). ES-MS $[M+H]^+$ calcd for $(C_{18}H_{17}N_4O_3)^+$: 337.1235, found: 337.1307.

*2.1.3.5. Ethyl 10-(4-methoxyphenyl)-8-methyl-2-phenyl-10H-pyrano [3,2-e][1,2,4]triazol[1,5-c]pyrimidine-9-carboxylate (**3e**).* White solid, yield 71%, mp: 171-173°C. ^{1}H NMR ($CDCl_3$, 300 MHz): δ (ppm) = 1.23 (t, 3H, H13, J= 7.0 Hz); 2.64 (s, 3H, H14); 3.72 (s, 3H, H15); 4.16 (q, 2H, H12, J= 7.0 Hz); 5.57 (s, 1H, H10); 6.81- 8.29 (m, 9H, Harom); 9.05 (s, 1H, H5). ^{13}C NMR ($CDCl_3$, 75 MHz): δ (ppm) = 14.1 (C13); 19.1 (C14); 37.0 (C10); 55.2 (C15); 60.7 (C12); 104.2 (C9); 107.2 (C10a); 113.7 (C3', 5'); 127.8 (C2'', 6''); 128.7 (C3'', 5''); 129.5 (C2', 6'); 129.7 (C4''); 130.9 (C1''); 135.1 (C1'); 138.1 (C5); 152.7 (C10b); 153.0 (C8); 158.7 (C4′); 159.6 (C2); 166.0 (C6a); 167.1 (C11). ES-MS $[M+H]^+$ calcd for $(C_{25}H_{23}N_4O_4)^+$: 443.1659, found: 443.1738.

*2.1.3.6. Ethyl 10-(4-methoxyphenyl)-2,8-dimethyl-10H-pyrano[3,2-e] [1,2,4]triazolo[1,5-c]pyrimidine-9-carboxylate (**3f**).* White solid, yield: 52%, mp: 168-170°C. ^{1}H NMR ($CDCl_3$, 300 MHz): δ (ppm) = 1.21 (t, 3H, H13, J= 5.2 Hz); 2.56 (s, 3H, H16); 2.60 (s, 3H, H14); 3.75 (s, 3H, H15); 4.13 (q, 2H, H12, J= 5.2 Hz); 5.47 (s, 1H, H10); 6.80 (d, H3′, 5′, J= 6.0 Hz); 7.36 (d, H2′, 6′, J= 6.0 Hz); 8.95 (s, 1H, H5). ^{13}C NMR ($CDCl_3$, 75 MHz): δ (ppm) = 14.0 (C13); 14.6 (CH3); 19.0 (CH3); 36.9 (C10); 55.2 (C15); 60.6 (C12); 104.0 (C9); 107.4 (C10a); 113.7 (C3', 5'); 129.4 (C2', 6'); 135.1 (C1'); 137.7 (C5); 152.6 (C10b); 152.8 (C2); 158.7 (C4′); 159.4 (C8); 165.9 (C6a); 167.3 (C11). ES-MS $[M+H]^+$ calcd for $(C_{20}H_{21}N_4O_4)^+$: 381.1485, found: 381.1518.

*2.1.3.7. Ethyl 10-(4-methoxyphenyl)-8-methyl-10H-pyrano[3,2-e] [1,2,4]triazolo[1,5-c] pyrimidine-9-carboxylate (**3g**).* White solid, yield: 62%, mp: 166-168°C. ^{1}H NMR ($CDCl_3$, 300 MHz): δ (ppm) = 1.23 (t, 3H, H13, J= 5.3 Hz); 2.61 (s, 3H, H14); 3.75 (s, 3H, H15); 4.15 (q, 2H, H12, J= 5.3 Hz); 5.49 (s, 1H, H10); 6.81 (d, H3′, 5′, J= 6.5 Hz); 7.35 (d, H2′, 6′, J= 6.5 Hz); 8.31 (s, 1H, H2);

9.10 (s, 1H, H5). ^{13}C NMR ($CDCl_3$, 75 MHz): δ (ppm) = 14.0 (C13); 19.0 (C14); 37.1 (C10); 55.1 (C15); 60.7 (C12); 104.6 (C9); 107.3 (C10a); 113.8 (C3', 5'); 129.4 (C2', 6'); 135.0 (C1'); 138.4 (C5); 152.1 (C10b); 152.8 (C2); 156.7 (C4'); 158.7 (C8); 159.2 (C6a); 165.8 (C11). ES-MS $[M+H]^+$ calcd for $(C_{19}H_{19}N_4O_4)^+$: 367.1328, found: 367.1362.

*2.1.3.8. Ethyl 10-(4-chlorophenyl)-8-methyl-2-phenyl-10H-pyrano[3,2-e][1,2,4]triazolo[1,5-c]pyrimidine-9-carboxylate (**3h**).* White solid, yield: 77%, mp: 218-220°C. ^{1}H NMR ($CDCl_3$, 300 MHz): δ (ppm) = 1.23 (t, 3H, H13, *J*= 5.3 Hz); 2.65 (s, 3H, H14); 4.15 (q, 2H, H12, *J*= 5.3 Hz); 5.58 (s, 1H, H10); 7.26 - 8.27 (m, 9H, Harom); 9.06 (s, 1H, H5). ^{13}C NMR ($CDCl_3$, 75 MHz): δ (ppm) = 14.0 (C13); 19.1 (C14); 37.4 (C10); 60.8 (C12); 103.4 (C9); 106.5 (C10a); 127.8 (C2', 6'); 128.5 (C2'', 6''); 128.7 (C3'', 5''); 129.6 (C3', 5'); 129.8 (C4''); 131.0 (C4'); 133.1 (C1''); 138.3 (C5); 141.2 (C1'); 152.6 (C10b); 152.9 (C8); 160.2 (C2); 165.7 (C6a); 167.2 (C11). ES-MS $[M+H]^+$ calcd for $(C_{24}H_{20}ClN_4O_3)^+$: 447.1146, found: 447.1176.

*2.1.3.9. Ethyl 10-(4-chlorophenyl)-2,8-dimethyl-10H-pyrano[3,2-e][1,2,4]triazolo[1,5-c] pyrimidine-9-carboxylate (**3i**).* White solid, yield: 56%, mp: 134-136°C. ^{1}H NMR ($CDCl_3$, 300 MHz): δ (ppm) = 1.22 (t, 3H, H13, *J*= 5.3 Hz); 2.57 (s, 3H, H15); 2.62 (s, 3H, H14); 4.15 (q, 2H, H12, *J*= 5.3 Hz); 5.50 (s, 1H, H10); 7.25 (d, H2′, 6′, *J*= 6.3 Hz); 7.40 (d, H3′, 5′, *J*= 6.3 Hz); 8.98 (s, 1H, H5). ^{13}C NMR ($CDCl_3$, 75 MHz): δ (ppm) = 14.0 (C13); 14.6 (CH_3); 19.1 (CH_3); 37.2 (C10); 60.8 (C12); 103.0 (C9); 106.8 (C10a); 128.6 (C2', 6'); 129.7 (C3', 5'); 133.1 (C4'); 138.0 (C5); 141.2 (C1'); 152.5 (C10b); 152.8 (C2); 160.0 (C8); 165.6 (C6a); 167.3 (C11). ES-MS $[M+H]^+$ calcd for $(C_{19}H_{18}ClN_4O_3)^+$: 385.0989, found: 385.0996.

*2.1.3.10. Ethyl 10-(4-chlorophenyl)-8-methyl-10H-pyrano[3,2-e][1,2,4]triazolo[1,5-c] pyrimidine-9-carboxylate (**3j**).* White solid, yield: 51%, mp: 188-190°C. ^{1}H NMR ($CDCl_3$, 300 MHz): δ (ppm) = 1.23 (t, 3H, H13, *J*= 5.2 Hz); 2.63 (s, 3H, H14); 4.15 (q, 2H, H12, *J*= 5.2 Hz); 5.53 (s, 1H, H10); 7.26 (d, H2′,6′, *J*= 6.1 Hz); 7.39 (d, H3′,5′, *J*= 6.1 Hz); 8.31 (s, 1H, H2); 9.12 (s, 1H, H5). ^{13}C NMR ($CDCl_3$, 75 MHz): δ (ppm) = 14.0 (C13); 19.0 (C14); 37.4 (C10); 60.9 (C12); 104.4 (C9); 106.8 (C10a); 128.6 (C2', 6'); 129.7 (C3', 5'); 133.2 (C4'); 138.6 (C5); 141.1 (C1'); 152.0 (C10b); 152.8 (C2); 156.7 (C8); 165.5 (C6a); 167.4 (C11). ES-MS $[M+H]^+$ calcd for $(C_{18}H_{16}ClN_4O_3)^+$: 371.0833, found: 371.0846.

2.2. In vitro α-amylase inhibition assay

α-Amylase inhibitory activity of synthesized compounds was determined using the assay method described by Kwon, Apostolidis and Shetty [24,25]. Briefly, 500 µL of each test sample at different concentrations was incubated with 500 µL of α-amylase solution (0.5 mg/mL in 0.02 M sodium phosphate buffer; pH 6.9 with 0.006 M NaCl). After pre-incubation at 25°C for 10 min, 500 µL of starch solution (1%) in 0.02 M sodium phosphate buffer (pH 6.9 with 0.006 M NaCl) was added to each tube. The resulting mixtures were then incubated at room temperature (10 min), and the reaction was stopped using 1 mL of DNS (Dinitro salicylic acid) reagent. At this time, the test tubes were placed in a water bath (100°C) for 5 min and cooled until room temperature was attained. The mixture was then diluted with 10 mL of deionized water, and the absorbance was determined at 540 nm. The readings were compared with the control, containing buffer instead of test compounds. Acarbose was used as a positive control. The inhibition of α-amylase was calculated using the following equation:

$$\%\text{inhibition of } \alpha - \text{Amylase} = \left(\text{Abs}_{\text{control}} - \text{Abs}_{\text{sample}}\right) / \left(\text{Abs}_{\text{control}}\right) \times 100$$

Where $\text{Abs}_{\text{control}}$ corresponds to the absorbance of the solution containing only α-amylase and the buffer instead of the compound, and $\text{Abs}_{\text{sample}}$ corresponds to the absorbance of the solution in the presence of both tested compound and α-amylase. Compound concentration providing 50% inhibition (IC_{50}) was obtained plotting the inhibition percentage against the concentrations of the tested compound. The tests were carried out in triplicate.

2.3. Molecular docking procedure

The 3D crystal structure of human pancreatic α-amylase (HPA) 2QV4.pdb was retrieved from the RCSB Protein Data Bank (http://www.rcsb.org/pdb/home/home.do). Water molecules, hetatoms, and other organic molecules were removed. The polar hydrogens and Gasteiger charges were then added to the HPA structure. The optimization of all chemical compounds structures was performed with ACD (3D viewer) software (http://www.filefacts.com/acd3d-viewer-freeware-info). The molecular docking analysis at the HPA-binding site was carried out using autodock Vina software [26,27]. Grid map of 40 × 40 × 40 Å dimensions with 1Å spacing was prepared using AutoGrid. The docking results were further analyzed using the Biovia Discovery Studio Visualizer v17.2.0.16349.

2.4. Computational details (DFT studies)

The entire set of calculations have been performed using DFT-B3LYP method with 6-311++G(d,p) basis set using Gaussian 09 program package [28] and GaussView visualization program [29]. HOMO–LUMO gaps of each compound were calculated by subtracting the LUMO energy value from the corresponding HOMO energy value. Different parameters have been determined such as chemical potential (μ), global hardness (η), global softness (S) and electrophilicity (ω) according to the following equations [30,31]:

$$\mu \cong (\text{EHOMO} + \text{ELUMO})/2;\ \eta \cong \text{ELUMO} - \text{EHOMO};\ \text{S} = 1/\eta;\ \omega = \mu^2/2\eta$$

3. Results and discussion

3.1. Chemistry

α-aminocarbonitriles constitute key precursors often used by chemists for the synthesis of a wide range of nitrogen molecules due to their high reactivity. Thereby, 2-amino- 3-cyanopyrane **1** was chosen as our starting material. It was prepared *via* one-pot three-component reaction of arylaldehyde, malononitrile, and ethyl acetoacetate according to some previous work [32]. Subsequently, our strategy for the target systems **3** was initially based on the construction of functionalized iminoether **2**, through the condensation reaction of precursor **1** with triethylorthoformate under reflux of acetic anhydride (Scheme 1).

Structures of compounds **1** and **2** were confirmed based on their spectral data. The ^{1}H NMR spectra of compounds **1** indicated essentially the presence of two singlets related to H_4 (δ_H 4.30-4.44) and NH_2 protons (δ_H 4.54-6.90). While examining the spectra of derivatives **2**, we observed the disappearance of amino group protons, the appearance of a singlet relative to the imidic proton and the presence of signals corresponding to a second ethoxy group. The ^{13}C NMR spectra of these precursors were in agreement with the proposed structures. Hence, the analysis of ^{13}C NMR spectra of iminoethers **2** showed mainly the appearance of new signals relative to carbons C_{13}, C_{12}, and the imidic carbon C_{11}.

Therefore, a series of new pyrano-triazolo-pyrimidine derivatives **3a-j** was prepared by cyclocondensation reaction of the intermediate **2** with appropriate hydrazides in the presence of a catalytic amount of acetic acid at reflux of dioxane (Scheme 2). Plausible pathway implies two successive nucleophilic additions of -NH2 group on the imidic carbon and on the nitrile function supervened

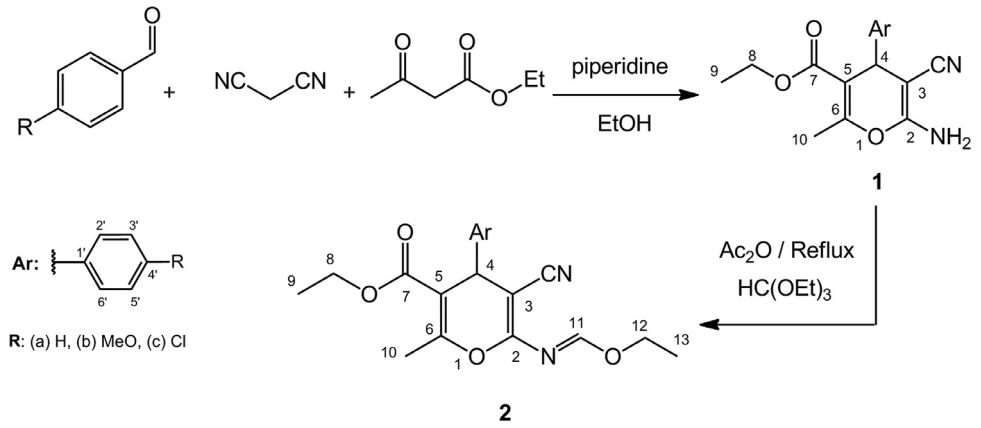

Scheme 1. Synthetic pathway to precursors **1** and **2**.

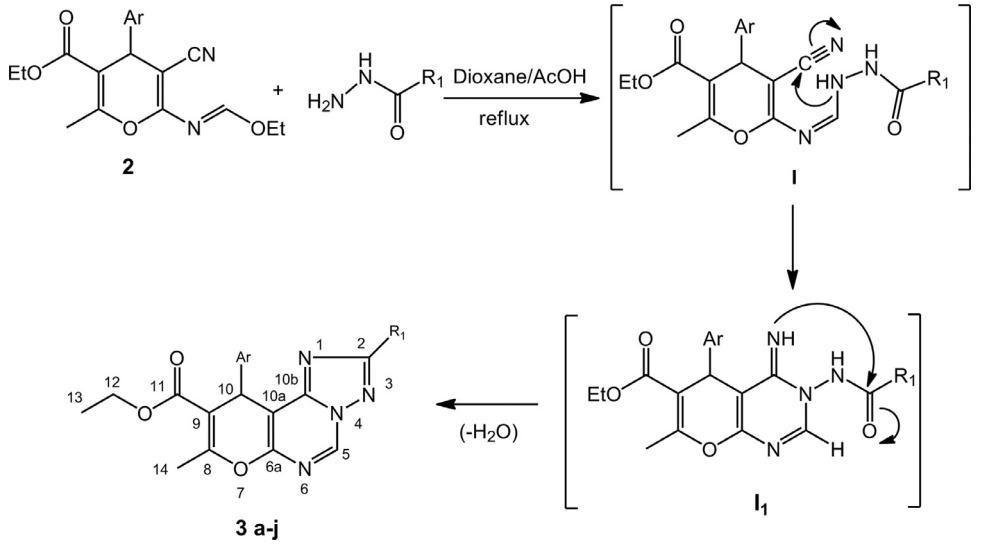

Scheme 2. Synthetic pathway to derivatives **3a-j**.

Table 1
Scope of hydrazides and the Ar functional group on **2** to synthesize compounds **3**.

	Ar	R_1	Yield (%)
3a	Ph	Ph	67
3b	Ph	CH_2CN	58
3c	Ph	CH_3	61
3d	Ph	H	54
3e	4-OCH_3Ph	Ph	71
3f	4-OCH_3Ph	CH_3	52
3g	4-OCH_3Ph	H	62
3h	4-ClPh	Ph	77
3i	4-ClPh	CH_3	56
3j	4-ClPh	H	51

by dehydrocyclization to obtain new heterocycles incorporating the pyran, triazole and pyrimidine nuclei **3** (Table 1).

Structures of the above compounds were established by spectroscopic methods. The ^{1}H NMR spectra of these compounds showed the disappearance of signals relative to the ethoxy group of the α-functionalized iminoether **2** and the presence of a singlet (8.95 - 9.12 ppm) corresponding to the imidic proton. The ^{13}C NMR spectra were also in agreement with the proposed structures and proved the presence of signals relative to C_5, C_{10b} carbons and those provided by the hydrazide used, in particular, carbon C_2. Further, the high-resolution mass spectra (ESI-HRMS) of all synthesized compounds have revealed the correct protonated molecular ion peaks $[M+H]^+$, which were compatible with the target structures.

3.2. In silico *pharmacokinetic prediction*

Pharmacokinetic (PK) properties are considered important factors in drug development since they define the characteristics of an effective oral drug. PKs are mainly related to the chemical descriptors of the molecule. Computer predictions are currently used in drug discovery programs to investigate an ADME profiling of new drug candidates to select only drug-like compounds with optimal PK [33]. Several physicochemical properties related to the pharmacokinetics of synthesized derivatives, were predicted for their compliance with Lipinski's rule of five using Molinspiration online software and SwissADME web tool [34–36]. As shown in Table 2, the prepared compounds were found to have Log P values less than five, implying good permeability across the cell membrane. It is one of the principal parameters for the estimation of lipophilicity of chemical compounds [20,37]. All the titled derivatives have weighted less than 500 and thereby predicting their easy transportation, absorption, and diffusion. It was observed also that the number of hydrogen bond acceptors and the number of hydrogen bond donors were less than 10 and 5, respectively. Interestingly, it can be anticipated that all products have good oral bioavailability as they obeyed Lipinski's rule of five [20]. The topological polar surface area (TPSA) is another significant factor in

Table 2
Prediction of physicochemical properties of the target compounds.

	TPSA[a]	n-rotb[b]	MW[c]	MV[d]	LogP[e]	n-OHNH[f]	n-ON[g]	Lipinski's violation
Rule			<500		<5	<5	<10	<1
1a	85.35	4	284.31	259.89	2.96	2	5	0
1b	94.59	5	314.34	285.43	3.02	2	6	0
1c	85.35	4	318.76	273.42	3.64	2	5	0
2a	80.93	7	340.38	314.21	3.77	0	6	0
2b	90.16	8	370.40	339.75	3.82	0	7	0
2c	78.63	7	374.82	327.74	4.45	0	6	0
3a	78.63	5	412.45	364.03	4.88	0	7	0
3b	102.42	5	375.39	326.28	2.84	0	8	0
3c	78.63	4	350.38	309.18	2.85	0	7	0
3d	78.63	4	336.35	292.62	2.77	0	7	0
3e	87.86	6	442.48	389.58	4.94	0	8	0
3f	87.86	5	380.40	334.73	2.91	0	8	0
3g	87.86	5	366.38	318.17	2.82	0	8	0
3h	78.63	5	446.89	377.57	4.89	0	7	0
3i	78.63	4	384.82	322.72	3.53	0	7	0
3j	78.63	4	370.80	306.16	3.45	0	7	0

[a] Topological polar surface area: TPSA.
[b] Num. of rotatable bonds: n-rotb.
[c] Molecular weight: MW.
[d] Molecular volume: MV.
[e] Logarithm of partition coefficient between n-octanol and water: LogP.
[f] Num. of hydrogen bond donors: n-OHNH.
[g] Num. of hydrogen bond acceptors: n-ON.

Table 3
Predicted ADME properties of the target compounds.

Compounds	BBB	PPB (%)	HIA (%)	Caco-2 (nm/sec)	hERG inhibition
1a	BBB +	76.82	95.85	19.89	WI
1b	BBB +	77.20	94.85	22.02	WI
1c	BBB +	88.49	97.46	21.37	WI
2a	BBB +	83.52	98.51	37.73	WI
2b	BBB +	81.73	98.04	43.20	WI
2c	BBB +	87.09	99.14	37.48	WI
3a	BBB +	99.13	97.92	41.77	WI
3b	BBB +	91.62	98.57	37.79	WI
3c	BBB +	86.81	99.07	34.60	WI
3d	BBB +	89.30	98.78	33.80	WI
3e	BBB +	97.22	98.48	45.82	WI
3f	BBB +	85.80	99.26	42.12	WI
3g	BBB +	89.83	99.14	36.63	WI
3h	BBB +	93.25	97.58	34.24	WI
3i	BBB +	88.74	98.53	29.05	WI
3j	BBB +	89.95	98.69	27.57	WI

**Blood-Brain Barrier (BBB): don't cross BBB (-); cross BBB (+),
Plasma protein binding (PPB): > 90 (strongly bound)
Human intestinal absorption (HIA, %): 70-100% (well absorbed)
Caco-2 cell permeability: < 4 (low permeability), 4-70 (medium permeability)
hERG inhibition: Human ether-a-go-go related gene channel inhibition; WI: Weak inhibitor

determining the molecular absorption rate. The number of rotatable bonds is also considered a good descriptor for suitable drugs. Their values for all compounds were in the normal range (TPSA values <140 Å^2 and n-rotb <10, as given in Table 2, according to Veber's rule [38]). ADME profile of synthesized derivatives was determined using PreADMET database. As indicated in Table 3, the absorption efficacy of all derivatives was found to be very high (94.85-99.26%) *via* the human intestinal tract. They have shown also medium permeability in the Caco-2 cell model and a positive result for blood-brain barrier crossing ability. Besides, the behavior of the drug depends on absorption and distribution which can be assessed by Plasma Protein Binding. Here, the molecules have displayed good binding affinity, especially compounds **3a, 3b, 3e**, and **3h**. Moreover, inhibition of potassium channels by the human ether-a-go-go related gene (hERG) leads mainly to QT syndrome with fatal ventricular arrhythmia [39]. In the present study, all prepared compounds showed a weak inhibitory property to the human hERG and are considered to be relatively safer. Toxicity parameters as mutagenicity, tumorigenicity, irritation, and reproductive or developmental toxicity of the synthesized components were estimated by OSIRIS Data Warrior [40]. Toxicity risk prediction softwares locate fragments within a molecule that represents a potential toxicity risk. The results indicated that none of the presented compounds contained any toxic subcomponents, which ensure the safety of all compounds (Table 4). From these various parameters, it can be concluded that the synthesized derivatives have shown strong drug-like performance and could be considered as promising candidates for further development.

3.3. In vitro α-amylase inhibitory activity

All the synthesized compounds (**1a**-**c**), (**2a**-**c**), and (**3a**-**j**) were subjected to *in vitro* α-amylase activity. The results, expressed in IC_{50} (μg/mL), are illustrated in the Table 5. Seven compounds **2a, 2b, 3a, 3b, 3c, 3e**, and **3h** exhibited interesting α-amylase inhibitory activity (IC_{50} = 9.58 ± 0.17 - 2.78 ± 0.14 μg/mL)

Table 4
Computational Toxicity Risk parameters.

	1a	1b	1c	2a	2b	2c	3a	3b	3c	3d	3e	3f	3g	3h	3i	3j
Mut	No	No	No	No	No	No	No	No	No	No	No	No	No	No	No	No
Tum	No	No	No	No	No	No	No	No	No	No	No	No	No	No	No	No
Irri	No	No	No	No	No	No	No	No	No	No	No	No	No	No	No	No
Rep	No	Low	No	No	Low	No	Low	No	No	No	Low	No	No	Low	No	No

Mut: Mutagenicity, Tumo: Tumorigenicity, Irri: Irritation, Rep: Reproductive or developmental toxicity.

Table 5
α-Amylase inhibitory activity of the synthesized compounds.[a]

Compound	IC_{50} (μg/mL)
1a	92.17 ± 1.52^{i}
1b	42.29 ± 1.10^{f}
1c	98.15 ± 2.42^{h}
2a	3.15 ± 0.25^{ab}
2b	3.28 ± 0.17^{ab}
2c	96.00 ± 3.74^{j}
3a	9.27 ± 0.15^{d}
3b	2.78 ± 0.14^{a}
3c	4.15 ± 0.10^{b}
3d	92.27 ± 2.50^{i}
3e	9.58 ± 0.17^{d}
3f	13.00 ± 1.11^{e}
3g	85.07 ± 2.88^{h}
3h	6.31 ± 0.09^{c}
3i	99.07 ± 3.08^{h}
3j	56.27 ± 2.12^{g}
Acarbose	6.84 ± 1.22^{c}

[a] Values given are the mean ± standard error. Different letters denote significant differences in IC_{50} values. Statistical significance was accepted at $P < 0.05$. IC_{50} was calculated using graph pad prism software.

compared to acarbose (IC_{50} = 6.84 ± 1.22 μg/mL). Compound **3b** (Ar= Ph and R1= CH_2CN) was found to be the most potent analog in this series (IC_{50} = 2.78 ± 0.14 μg/mL). The rest of compounds displayed moderate to weak activity. It has been found that the iminoethers **2a** and **2b** exhibited good and comparable inhibitory potency with a IC_{50} values of 3.15 ± 0.25 and 3.28 ± 0.17 μg/mL, respectively, while the starting compounds **1a** and **1b** displayed relatively less activity (IC_{50} = 92.17 ± 1.52 and 42.29 ± 1.10 μg/mL, respectively). This implies the importance of modifying the primary amine function to an imine. Regarding the series **3a-j**, the first suggestion is that the incorporation of the pyrimidine and triazole rings has significantly improved the activity compared to the starting reagents (**1a-c**) which showed limited inhibition of the enzyme. The nature of the aryl moiety and the substituents on the triazole ring (R_1) may influence the inhibitory potential. The results showed that in the series **3a-d** (Ar= Ph), the highest activity was noted when R1= CH_2CN (case of **3b**). For the series **3e-3g** (Ar= 4-OCH_3Ph), the activity is better with R1 = Ph (case of **3e**, IC_{50} = 9.58 ± 0.17 μg/mL) and for the series **3h-3j** (Ar= 4-ClPh), the most active derivative was found to be **3h** with R1= Ph (IC_{50} = 6.31 ± 0.09 μg/mL).

The presence of a CH_2CN group linked to the triazole ring in **3b** could better facilitate its interaction with the enzyme compared to the phenyl, methyl and hydrogen in the rest derivatives. Such results highlight the importance of the nature of the substituent carried by the triazole.

3.4. Molecular docking analysis

To predict the putative binding mode of the active derivatives with the target protein α-amylase, a docking study was carried out into the active site of co-crystal structure PDB: 2QV4, using Autodock Vina. The docking results of tested inhibitors revealed that the seven synthesized ligands displayed a various type of intermolecular interactions with the significant residues of the active site (Trp 58, Trp 59, Tyr 62, Gln 63, Tyr 151, Leu 162, Leu 165, Asp 197, Ala 198, Lys 200, His 201, Glu 233, Ile 235, Asp 300 and His 305) of the target enzyme [41]. In the first instance, we re-docked the co-crystallized ligand (acarbose) in the binding site of α-amylase with the same parameters as used for the docking of synthesized ligands. The co-crystallized ligand showed seven hydrogen bond interactions with the amino-acid residues Trp 59, Ala 106, Gly 164, Asp 197, Asp 300, and His 305 of the target enzyme (Fig. 3). The value of the binding energy of acarbose was found to be −7.6 kcal/mol. Analysis of the best-docked poses of iminoethers **2a** and **2b** revealed that they mainly exhibited hydrogen and hydrophobic interactions. As shown in figure S1, the ethoxy group's oxygen linked to the imine function and the pyran ring of compound **2a** have established conventional and Pi-Donor hydrogen bonds with His 305 and Tyr 151, respectively. Additionally, the pyran, phenyl ring, and methyl group of conjugate **2a** have interacted through hydrophobic interactions (Pi-Sigma, Pi-Pi T-shaped, and Pi-Alkyl) with Ile 235, Tyr 151, His 201, Leu 162, Lys 200, and Ala 198. It was noteworthy that the pyran nucleus, in compound **2b**, was involved in an electrostatic interaction with Asp 300, which can play an essential role in stabilizing the inhibitor in the active site.

Further, compound **3b** demonstrated the highest activity in the series, displayed numerous strong interactions through residues that are present on the side chain of the active site of α-amylase, exhibiting binding energy -8.0 kcal/mol. Interestingly, the amino acid residues Gln 63 has formed Hydrogen donor interaction with the cyano-group nitrogen (3.00 Å), which stabilizes its binding affinity with the target receptor, and may therefore be responsible for its significant *in vitro* activity. This product was also found to exhibit crucial hydrophobic contacts: three Pi-Alkyl, a Pi-Pi T-shaped, and three alkyl interactions with His 201, Leu 162, Leu 165, Tyr 62, Ala 198, Leu 162, Ile 235, respectively (Fig. 4).

Binding manner of **3c,** the second most active derivative in the series **3**, revealed that this compound was involved in numerous interactions including Hydrogen Bond, Pi-anion, Pi-sigma, Pi-Pi T-Shaped, and Pi-alkyl interactions with the side chain residues Tyr 151, Glu233, Ile235, His201, Lys200, and Leu162. These interactions could be the main reason for stabilizing the inhibitor-receptor complex and making the derivative second most active analog among the series. Similarly, hydrophobic interactions and hydrogen bindings (especially with residue Lys 200), were found as well in the case of compounds **3a, 3e**, and **3h**. Electrostatic bonds were also observed, in the conjugates **3a** and **3h**, with residues Asp 197 and Glu 233 (Fig. S2, **3h** as an example) that may explain the lower binding energy values of these compounds compared to acarbose: -8.9 and -9.2 Kcal/mol, respectively (Table 6).

3.5. Density functional theory (DFT)-based computations: frontier molecular orbital analysis

DFT-based computation could potentially be an effective tool in computer-aided drug design and thus, becoming an attractive method for medicinal studies [42]. The energies of frontier molec-

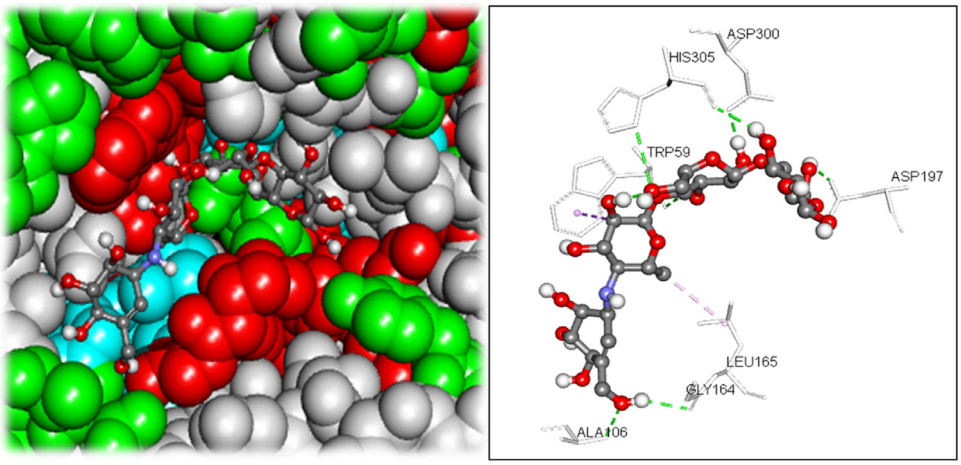

Fig. 3. 3D-representation of the docked pose of the co-crystallized ligand (Acarbose) in the active site of α-amylase.

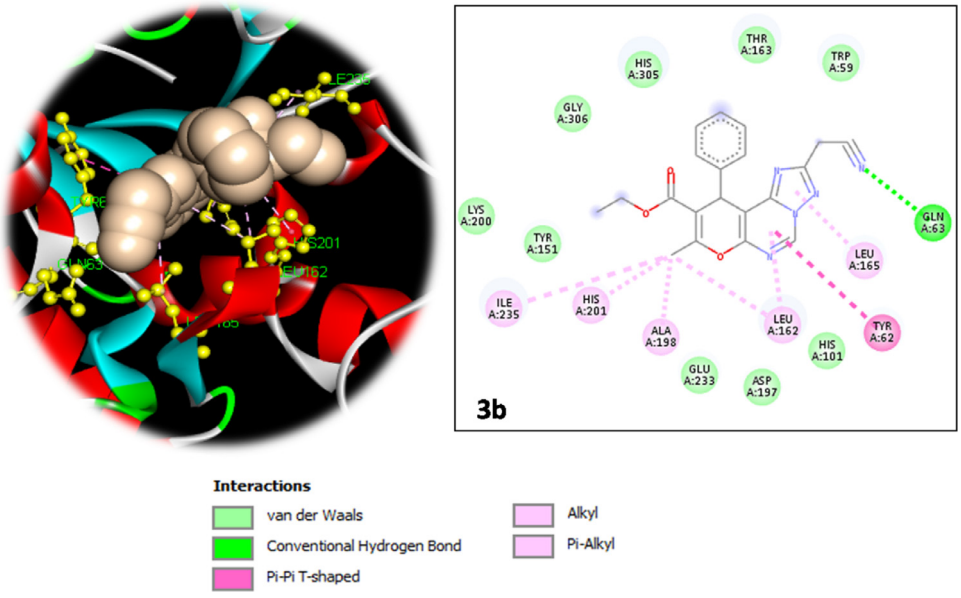

Fig. 4. Predicted binding modes of conjugate **3b** in the active site of α-amylase (PDB: 2QV4).

Table 6
Binding Energies of tested compounds with α-amylase enzyme (2QV4).

Compound	Binding energy (kcal/mol)
2a	-7.7
2b	-7.4
3a	-8.9
3b	-8.0
3c	-7.4
3e	-9.4
3h	-9.2
Acarbose	-7.6

ular orbitals are significant parameters in various chemical and pharmacological processes.

The highest occupied molecular orbital energy EHOMO measures the electron-donating character of a compound, while the lowest unoccupied molecular orbital energy ELUMO assesses its electron-accepting character. HOMO and LUMO orbitals can be used to explain different types of reactions and predict the most reactive position in conjugated systems [43]. The energy gap between HOMO and LUMO is responsible for the stability of the molecule. Molecules with a larger EHOMO-LUMO band gap should be more stable than those having a smaller gap [44]. As indicated in Table 7, **3a**, **3e**, and **3h** show the three lowest energy gap values (2.901, 2.918, and 2.912 eV, respectively), suggesting that they are more reactive and less stable compared to the rest of the compounds.

The HOMO and LUMO distributions of the active derivatives (**2a, 2b, 3a, 3b, 3c, 3e**, and **3h**) are illustrated in Figs. 5, S3, and S4. The localization pattern of frontier molecular orbitals in different positions demonstrates their structural and functional diversity.

As can be seen from figures (5, S3 and S4), strong delocalization of the HOMO for compounds **2a** and **2b** occurs on the pyranic nucleus, nitrile, and imine groups (donors moieties) while strong delocalization of the LUMO occurs on the benzene ring (acceptor moiety). Further, strong delocalization of the HOMO for the other compounds occurs on the pyranotriazolopyrimidine donor moiety while strong delocalization of the LUMO occurs on the benzene ring bonded to triazole (**3a, 3e**, and **3h**) and on the benzene ring attached to pyran (**3b** and **3c**). Thus, the lowering of the HOMO-LUMO E-gap is mainly a consequence of the high stabilization of the LUMO owing to the high electron-accepting capacity of the electron acceptor group.

Table 7
DFT/B3LYP/6–311++G(d,p) calculations of HOMO-LUMO energy gap, chemical potential, global hardness, global softness, electrophilicity index and dipole moment of compounds **1, 2** and **3**.

	E_{HOMO}(eV)	E_{LUMO}(eV)	ΔE(eV)	μ (eV)	H(eV)	S $(eV)^{-1}$	ω(eV)	D. M (Debye)
1a	-8.135	-4.725	3.410	-6.430	3.410	0.292	6.063	6.882
1b	-8.124	-4.622	3.501	-6.373	3.501	0.286	5.801	7.620
1c	-8.017	-4.630	3.384	-6.324	3.384	0.294	5.906	7.502
2a	-8.241	-4.838	3.403	-6.541	3.403	0.294	6.286	4.349
2b	-8.240	-4.711	3.526	-6.476	3.526	0.282	5.945	3.392
2c	-8.040	-4.728	3.311	-6.384	3.311	0.302	6.152	4.948
3a	-7.975	-5.073	2.901	-6.524	2.901	0.345	7.331	2.285
3b	-7.991	-4.763	3.230	-6.376	3.230	0.310	6.295	5.566
3c	-7.992	-4.760	3.232	-6.375	3.232	0.308	6.290	2.229
3d	-8.011	-4.762	3.246	-6.386	3.246	0.308	6.280	3.026
3e	-7.978	-5.060	2.918	-6.519	2.918	0.343	7.281	3.088
3f	-7.993	-4.656	3.339	-6.325	3.339	0.299	5.990	2.223
3g	-8.012	-4.646	3.365	-6.329	3.365	0.297	5.944	3.907
3h	-7.976	-5.064	2.912	-6.521	2.912	0.342	7.296	2.946
3i	-7.991	-4.654	3.337	-6.322	3.337	0.299	5.989	3.019
3j	-8.010	-4.660	3.350	-6.335	3.350	0.297	5.988	3.739

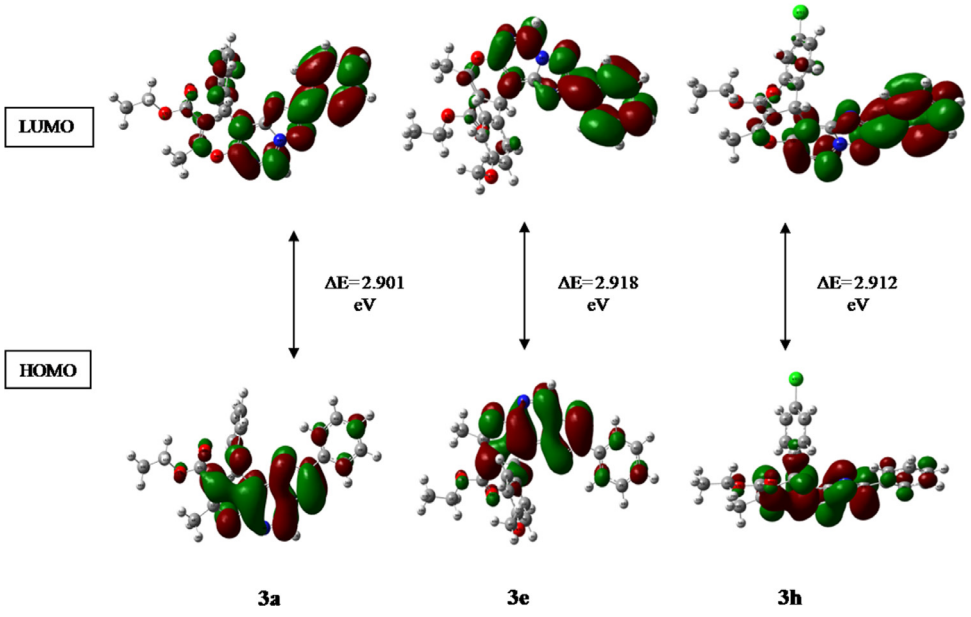

Fig. 5. Visualization of frontier molecular orbitals of **3a, 3e** and **3h** with DFT/B3LYP method using 6-311++G(d,p) basis set.

Moreover, HOMO-LUMO energy values are the basis for calculating some global chemical reactivity parameters such as chemical potential (μ), global hardness (η), global softness (S), electrophilicity index (ω) and dipole moment (D.M). These quantum chemical descriptors, computed at B3LYP/6-311++G(d,p) level, are presented in Table 7.

Therefore, the energy gap of HOMO–LUMO is used to determine the hardness and the softness of the molecules. Large gaps denote a hard molecule and small gaps signify a soft molecule. Softness is defined as the reciprocal of hardness and hence, the reactivity of a molecule rises with the increase in the softness [45]. **3a, 3e**, and **3h** show the lowest values of chemical hardness and energy gap, and so, the three highest softness values (0.345, 0.343, and 0.342 eV, respectively), proving that they are softer and most reactive species.

The dipole moment is another significant electronic parameter that is due to the non-uniform distribution of charges on the different atoms in a given molecule [46]. It is an indicator of drug-receptor interaction, which facilitates hydrogen-bond interactions [33,47]. All synthesized compounds show comparatively higher dipole moments varying from 2.223 to 7.620 Debey. The values of the dipole moment promote intermolecular interactions. Besides, the global electrophilicity index provides information about stability (hardness) and also the electron transfer (chemical potential) and is an effective descriptor of global chemical reactivity. It is useful for explaining the binding capacity with biomolecules [48,49]. The higher electrophilicity index of studied compounds (especially **3a** (7.331 eV), **3e** (7.281 eV), and **3h** (7.296 eV)), will have higher binding interactions.

4. Conclusion

In this paper, we have synthesized a series of new pyranotriazolopyrimidine **3a-j** by reacting the α-functionalized-iminoether **2**, previously prepared from α-aminocarbonitrile **1**, with a series of hydrazides. Pharmacokinetics and toxicological predictions have revealed their drug-like properties, presenting good ADMET properties and showing good oral bioavailability as they obeyed Lipinski's rule of five. The newly prepared compounds **1-3** have been tested for *in vitro* α-amylase activity. Among them, **2a, 2b, 3a, 3b, 3c, 3e**, and **3h** exhibited interesting α-amylase inhibitory activity, and **3b** was found to be the most active one (IC_{50}= 2.78 ± 0.14 mg/mL). *In silico* studies were performed to gain insight toward the interactions of title compounds with the target protein. The bind-

ing modes of active compounds showed that hydrophobic and hydrogen bonds interactions with important residues such as Gln 63, Tyr 151, Leu 162, Leu 165, Asp 197, Ala 198, Lys 200, His 201, Glu 233, Ile 235, Asp 300, and His 305, appeared significant for high potency. A theoretical DFT/B3LYP study has been carried out to explain the reactivity of the different compounds. The use of the reactivity parameters of HOMO-LUMO energies has been discussed. As we saw, **3a, 3e**, and **3h** showed the lowest values of chemical hardness, energy gap, and the three highest softness values, in comparison with the other molecules, making them the most reactive species in the series. This study will be useful for further lead optimization and developing new α-amylase inhibitors.

Author Statement

Amel Hajlaoui did the synthesis work and the Docking party. Maha Laajimi performed the DFT study. Mansour Znati tested the α-amylase activity. Hichem Ben Jannet contributed to the discussion of the results and completed the redaction of the manuscript. Anis Romdhane was the supervisor of the present work, he also checked the structure determination of the synthesized compounds and the biological study, and he completed the redaction of the article.

Declaration of Competing Interest

The authors declare that they have no known competing financial interests or personal relationships that could have appeared to influence the work reported in this paper.

Supplementary materials

Supplementary material associated with this article can be found, in the online version, at doi:10.1016/j.molstruc.2021.130346.

References

[1] G. Wang, Z. Peng, J. Wang, X. Li, J. Li, Synthesis, *in vitro* evaluation and molecular docking studies of novel triazine-triazole derivatives as potential α-glucosidase inhibitors, Eur. J. Med. Chem. 125 (2017) 423–429.

[2] H. Kashtoh, M.T. Muhammad, J.J.A. Khan, S. Rasheed, A. Khan, S. Perveen, K. Javaid, K.M.Khan Atia-tul-Wahab, M.I. Choudhary, Dihydropyrano [2,3-*c*] pyrazole: Novel *in vitro* inhibitors of yeast α-glucosidase, Bioorg. Chem. 65 (2016) 61–72.

[3] R. Tundis, M.R. Loizzo, F. Menichini, Natural Products as α-Amylase and α-Glucosidase Inhibitors and their Hypoglycaemic Potential in the Treatment of Diabetes: An Update, Mini-Rev. Med. Chem. 10 (2010) 315–331.

[4] R.R. Ruddarraju, G. Kiran, A.C. Murugulla, R. Maroju, D.K. Prasad, B.H. Kumar, V. Bakshi, N.S. Reddy, Design, synthesis and biological evaluation of theophylline containing variant acetylene derivatives as α-amylase inhibitors, Bioorg. Chem. 92 (2019) 103–120.

[5] M.S. Ganesan, K.K. Raja, K. Narasimhan, S. Murugesan, B.K. Kumar, Design, synthesis, α-amylase inhibition and *in silico* docking study of novel quinoline bearing proline derivatives, J. Mol. Struct. 1208 (2020) 127873.

[6] R. Rafique, K.M. Khan, Kanwal Arshia, S. Chigurupati, Abdul Wadood, A. Ur Rehman, A. Karunanidhi, S. Hameed, M. Taha, M. al-Rashida, Synthesis of new indazole based dual inhibitors of α-glucosidase and α-amylase enzymes, their *in vitro, in silico* and kinetics studies, Bioorg. Chem. 94 (2020) 103–195.

[7] M. Dhamej, P. Gupta, Synthetic heterocyclic candidates as promising α-glucosidase inhibitors: An overview, Eur. J. Med. Chem. 176 (2019) 343–377.

[8] T. Umar, S. Gusain, M.K. Raza, S. Shalini, J. Kumar, M. Tiwari, N. Hoda, Naphthalene-triazolopyrimidine hybrid compounds as potential multifunctional anti-Alzheimer's agents, Bioorg. Med. Chem. 27 (2019) 3156–3166.

[9] M. Cherif, M. Horchani, Y.O. Al-Ghamdi, S.G. Almalki, Y.E. Alqurashi, H.Ben Jannet, A. Romdhane, New prano-1,2,3-triazolopyrimidinone derivatives as anticholinesterase and antibacterial agents: Design, microwave-assisted synthesis and molecular docking study, J. Mol. Struct. 1220 (2020) 128685.

[10] F. Panahi, R. Yousefi, M.H. Mehraban, A.K. Nezhad, Synthesis of new pyrimidine-fused derivatives as potent and selective antidiabetic α-glucosidase inhibitors, Carbohydr. Res. 380 (2013) 81–91.

[11] A. Romdhane, A. Ben Said, M. Cherif, H. Ben Jannet, Design, synthesis and anti-acetylcholinesterase evaluation of some new pyrazolo[4,3-e]-1,2,4-triazolo[1,5-c]pyrimidine derivatives, Med. Chem. Res. 25 (2016) 1358–1368.

[12] P. Yadav, K. Lal, L. Kumar, A. Kumar, A. Kumar, A.K. Paul, R. Kumar, Designed chalcone-1,2,3-triazole conjugates as potential antimicrobial agents synthesis, crystal structure and antimicrobial potential of some fluorinated chalcone-1,2,3-triazole conjugates, Eur. J. Med. Chem. 155 (2018) 263–274.

[13] A. Maleki, Z. Varzi, F. Hassanzadeh-Afruzi, Preparation and characterization of an eco-friendly ZnFe2O4@alginic acid nanocomposite catalyst and its application in the synthesis of 2-amino-3-cyano-4*H*-pyran derivatives, Polyhedron 171 (2019) 193–202.

[14] D. Kumar, P. Sharma, H. Singh, K. Nepali, G.K. Gupta, S.K. Jaina, F. Ntie-Kang, The value of pyrans as anticancer scaffolds in medicinal chemistry, RSC Adv. 7 (2017) 36977–36999.

[15] M. Zayane, A. Rahmouni, M.D. Remadi, M. Ben Mansour, A. Romdhane, H.Ben Jannet, Design and synthesis of antimicrobial, anticoagulant, and anticholinesterase hybrid molecules from 4-methylumbelliferone, J. Enzyme Inhib. Med. Chem. 31 (2016) 1566–1575.

[16] Y. Bouazizi, A. Romdhane, H.Ben Jannet, Synthesis of new 3,4-dihydropyrano[c]chromene derivatives and their evaluation as acetyl cholinesterase inhibitors, Eur. J. Chem. 5 (2014) 457–462.

[17] B. Maleki, M. Baghayeri, S.A.J. Abadi, R. Tayebee, A. Khojastehnezhad, Ultrasound Promoted Facile One Pot Synthesis of Highly Substituted Pyran Derivatives Catalyzed by Silica-Coated Magnetic NiFe2O4 Nanoparticles-Supported $H_{14}[NaP_5W_{30}O_{110}]$ under Mild Conditions, **RSC Adv** 6 (2016) 96644–96661.

[18] S. Wang, Q. Qi, C. Li, G. Ding, S.H. Kim, Photoswitching of bisthienylethene using 2D-π-A type pyran-based fluorescent dye for rewritable optical storage, Dyes Pigm 89 (2011) 188–192.

[19] S. Hameed, F.Seraj Kanwal, R. Rafique, S. Chigurupati, Abdul Wadood, A. Ur Rehman, V. Venugopal, U. Salar, M. Taha, K.M. Khan, Synthesis of benzotriazoles derivatives and their dual potential as α-amylase and α-glucosidase inhibitors *in vitro*: Structure-activity relationship, molecular docking, and kinetic studies, Eur. J. Med. Chem. 183 (2019) 111677.

[20] P.A. Channar, A. Saeed, F.A. Larik, S. Rashid, Q. Iqbal, M. Rozi, S. Younis, J. Mahar, Design and synthesis of 2,6-di(substituted phenyl)thiazolo[3,2-b]-1,2,4-triazoles as α-glucosidase and α-amylase inhibitors, co-relative Pharmacokinetics and 3D QSAR and risk analysis, Biomed. Pharmacother. 94 (2017) 499–513.

[21] H. Kashtoh, M.T. Muhammad, J.J.A. Khan, S. Rasheed, A. Khan, S. Perveen, K. Javaid, K.M.Khan Atia-tul-Wahab, M.I. Choudhary, Dihydropyrano [2,3-*c*] pyrazole: Novel *in vitro* inhibitors of yeast α-glucosidase, Bioorg. Chem. 65 (2016) 61–72.

[22] A. Yousefi, R. Yousefi, F. Panahi, S. Sarikhani, A. Zolghadr, A. Bahaoddini, A. Khalafi-Nezhad, Novel curcumin-based pyrano[2,3-d]pyrimidine anti-oxidant inhibitors for α-amylase and α-glucosidase: Implications for their pleiotropic effects against diabetes complications, Int. J. Biol. Macromol. 78 (2015) 46–55.

[23] M. Amirnejad, M.R. Naimi-Jamal, H. Tourani, H. Ghafuri, A facile solvent-free one-pot three-component method for the synthesis of 2-amino-4*H*-pyrans and tetrahydro-4*H*-chromenes at ambient temperature, Monatsh. Chem. 144 (2013) 1219–1225.

[24] Y.-I. Kwon, E. Apostolidis, K. Shetty, *In vitro* studies of eggplant (Solanum melongena) phenolics as inhibitors of key enzymes relevant for type 2 diabetes and hypertension, Bioresour. Technol. 99 (2008) 2981–2988.

[25] Z. Toobaei, R. Yousefi, F. Panahi, S. Shahidpour, M. Nourisefat, M.M. Doroodmand, A. Khalafi-Nezhad, Synthesis of novel poly-hydroxyl functionalized acridine derivatives as inhibitors of α-Glucosidase and α-Amylase, Carbohydr. Res. 411 (2015) 22–32.

[26] O. Trott, A.J. Olson, Software News and Update AutoDock Vina: Improving the Speed and Accuracy of Docking with a New Scoring Function, Efficient Optimization, and Multithreading, J. Comput. Chem. 31 (2010) 455–461.

[27] http://autodock.scripps.edu/

[28] M.J. Frisch, G.W. Trucks, H.B. Schlegel, et al., Gaussian 09, Revision B.01, Gaussian, Inc., Wallingford, CT, 2010.

[29] R.I. Dennington, T. Keith, J. Millam, GaussView, Version 5.0.8, Semichem. Inc. Shawnee Mission, KS, 2008.

[30] S. Chortani, H. Edziri, M. Manachou, Y.O. Al-Ghamdi, S.G. Almalki, Y.E. Alqurashi, H.Ben Jannet, A. Romdhane, Novel 1,3,4-oxadiazole linked benzopyrimidinones conjugates: Synthesis, DFT study and antimicrobial evaluation, J. Mol. Struct. 1217 (2020) 128357.

[31] L.R. Domingo, M. Ríos-Gutiérrez, P. Pérez, Applications of the Conceptual Density Functional Theory Indices to Organic Chemistry Reactivity, Molecules 21 (2016) 748.

[32] A. Romdhane, H.Ben Jannet, Synthesis of new pyran and pyranoquinoline derivatives, Arab. J. Chem. 10 (2017) S3128–S3134.

[33] M. Shahinozzaman, N. Taira, T. Ishii, M.A. Halim, M.A. Hossain, S. Tawata, Anti-Inflammatory, Anti-Diabetic, and Anti-Alzheimer's Effects of Prenylated Flavonoids from Okinawa Propolis: An Investigation by Experimental and Computational Studies, Molecules 23 (2018) 2479.

[34] Z. Lv, W. He, X. Tian, J. Kang, Y. Liu, Y. Peng, L. Zheng, Q. Wang, W. Yu, J. Chang, Design, synthesis, and biological evaluation of new N^4-Substituted 2'-deoxy-2'-fluoro-4'-azido cytidine derivatives as potent anti-HBV Agents, Eur. J. Med. Chem. 101 (2015) 103–110.

[35] C.A. Lipinski, F. Lombardo, B.W. Dominy, P.J. Feeney, Experimental and computational approaches to estimate solubility and permeability in drug discovery and development settings, Adv. Drug Deliv. Rev. 23 (1997) 3–25.

[36] A. Daina, O. Michielin, V. Zoete, SwissADME: a free web tool to evaluate pharmacokinetics, druglikeness and medicinal chemistry friendliness of small molecules, Sci. Rep. 7 (2017) 42717.

[37] J. Ashraf, E.U. Mughal, A. Sadiq, N. Naeem, S.A. Muhammad, T. Qousain, M.N. Zafar, B.A. Khan, M. Anees, Design and synthesis of new flavonols as dual α-amylase and α-glucosidase inhibitors: Structure-activity relationship, drug–likeness, *in vitro* and *in silico* studies, J. Mol. Struct. 1218 (2020) 128458.
[38] D.F. Veber, S.R. Johnson, Hung-Yuan Cheng, B.R. Smith, K.W. Ward, K.D. Kopple, Molecular Properties That Influence the Oral Bioavailability of Drug Candidates, J. Med. Chem. 45 (2002) 2615–2623.
[39] M.M. Matin, M.S. Hasan, M. Uzzaman, M.M.H. Bhuiyan, S.M. Kibria, M.E. Hossain, M.H.O. Roshid, Synthesis, spectroscopic characterization, molecular docking, and ADMET studies of mannopyranoside esters as antimicrobial agents, J. Mol. Struct. 1222 (2020) 128821, doi:10.1016/j.molstruc.2020.128821.
[40] T. Sander, J. Freyss, M. von Korff, C. Rufener, DataWarrior: An Open-Source Program For Chemistry Aware Data Visualization And Analysis, J. Chem. Inf. Model. 55 (2015) 460–473.
[41] K. Rehman, T.A. Chohan, I. Waheed, Z. Gilani, M.S.H. Akash, Taxifolin prevents postprandial hyperglycemia by regulating the activity of α-amylase: Evidence from an *in vivo* and *in silico* studies, J. Cell. Biochem. 120 (2019) 425–438.
[42] H. Tandon, T. Chakraborty, V. Suhag, A Brief Review on Importance of DFT In Drug Design, Res Med Eng Sci 7 (2019) 791–795.
[43] N. Choudhary, S. Bee, A. Gupta, P. Tandon, Comparative vibrational spectroscopic studies, HOMO–LUMO and NBO analysis of *N*-(phenyl)-2,2-dichloroacetamide, *N*-(2-chloro phenyl)-2,2-dichloroacetamide and *N*-(4-chloro phenyl)-2,2-dichloroacetamide based on density functional theory, Comput. Theor. Chem. 1016 (2013) 8–21.
[44] B. Amul, S. Muthu, M. Raja, S. Sevvanthi, Spectral, DFT and molecular docking investigations on Etodolac, J. Mol. Struct. 1195 (2019) 747–761.
[45] F. Azam, N.H. Alabdullah, H.M. Ehmedat, A.R. Abulifa, I. Taban, S. Upadhyayula, NSAIDs as potential treatment option for preventing amyloid β toxicity in Alzheimer's disease: an investigation by docking, molecular dynamics, and DFT studies, J Biomol Struct Dyn 36 (2017) 2099–2117.
[46] A.M. Mansour, N.T. Abdel Ghani, Hydrogen-bond effect, spectroscopic and molecular structure investigation of sulfamethazine Schiff-base: Experimental and quantum chemical calculations, J. Mol. Struct. 1040 (2013) 226–237.
[47] E.J. Lienx, Z-Ru Guo, R-Li Li, C-Tang Su, Use of Dipole Moment as a Parameter in Drug-Receptor Interaction and Quantitative Structure-Activity Relationship Studies, J. Pharm. Sci. 71 (1982) 641–655.
[48] S. Alyar, Tü. Şen, C. Şen, H. Alyar, Ş. Adem, Üü.Ö. Özdemir, Synthesis, spectroscopic characterizations, enzyme inhibition, molecular docking study and DFT calculations of new Schiff bases of sulfa drugs, J. Mol. Struct. 1185 (2019) 416–424.
[49] R. Parthasarathi, V. Subramanian, D.R. Roy, P.K. Chattaraj, Electrophilicity index as a possible descriptor of biological activity, Bioorg. Med. Chem. 12 (2004) 5533–5543.